Torrefaction of Almond and Walnut Byproducts

Zach McCaffrey[1]*, Lennard Torres[1], Bor-Sen Chiou[1], Saulo Rocha Ferreira[2],
Luiz Eduardo Silva[3], Delilah F. Wood[1] and William John Orts[1]

[1] Bioproducts Research Unit, Western Regional Research Center (WRRC), United States Department of Agriculture (USDA), Albany, CA, United States, [2] Civil Engineering Department, Federal University of Lavras, Lavras, Brazil, [3] Forest Science Department, Federal University of Lavras, Lavras, Brazil

While the US nut industry is growing, markets for nut by-products, particularly nutshells and tree prunings, have not kept pace. Torrefaction is a thermochemical process used to improve physicochemical properties of biomass for energy and other applications. The goal of the paper was to characterize the effects of a range of torrefaction conditions on the properties of nut by-product feedstock. The process consists of thermal treatment of biomass at a temperature between 200 and 300°C in the absence of oxygen, where final material properties of the torrefied biomass depend on the temperature, heating rate, and residence time. In general, torrefied biomass exhibits higher hydrophobicity and calorific value with reduced moisture absorption compared to untreated biomass, making it an ideal fuel source for energy applications compared to raw biomass. In this study, almond shells of soft, semi-soft, and hardshell varieties, as well as walnut shells and almond wood, were torrefied at two different temperatures (230 and 290°C) and three different residence times (20, 40, and 60 min) in order to characterize the physicochemical properties. The thermal behavior of raw and heat-treated biomass was investigated by TGA analysis, elemental analysis, pH, helium pycnometry, FTIR spectroscopy, and dynamic vapor sorption analysis.

Keywords: torrefaction, almond shells, walnut shells, almond wood, biomass power

INTRODUCTION

Interest in the application of biomass torrefaction as a method for modifying material is increasing. Depending on the feedstock and the application, it may be advantageous to target particular material properties, e.g., density, calorific value, moisture sorption, grindability, etc. The diverse range of torrefied biomass material properties depends on its physicochemical properties, which depend on the thermal processing conditions (i.e., temperature and residence time) and properties of the original feedstock. Thus, detailed information about the thermal processes are important for optimizing biomass material properties to a specific application (Fuad et al., 2019; Yan et al., 2021). Torrefaction is a thermal process in which temperature is maintained between 200 and 300°C in a low-oxygen environment. The heat-treatment process first removes most of the inherent hemicellulose and amorphous cellulose in the biomass but leaves the lignin mostly intact (Melkior et al., 2012). Products of biomass torrefaction include: (1) a permanent gas, composed mostly of CO_2 and CO; (2) a condensable liquid, which is composed mostly of water, organic acids,

aldehydes, and phenolic compounds; and (3) a carbonized solid, referred to as torréfied biomass. The liquid condensate, composed of organic acids, aldehydes and phenolic compounds, can theoretically be a source for chemical products after separation (Doddapaneni et al., 2018). However, in practice there are alternative established processes that are more reliable and cost efficient (Stelte, 2012). Without separation, the condensate has potential use as an herbicide, pesticide, fungicide, insecticide, and repellent (Fagernas et al., 2015). Typically, the torréfied biomass results in solid yields of over 50% (Chen et al., 2018).

Biomass feedstock for torrefaction can come from a variety of sources. One such source comes from the nut agricultural industries. Nut production has increased tremendously in the United States since 1980 (**Figure 1**); however, traditional markets for their by-products—the cattle and chicken feed market, for example—have not kept pace. The US produces 82% of the world's almonds (estimated at 839 million kilograms of kernels for 2019) and 31% of the world's walnuts, resulting in nearly 2.25 billion kilograms of almond hulls, 635 million kilograms of almond shells, and over 320 million kilograms of walnut shells with almost no market outlets (Almond Board of California, 2018; International Nuts & Dried Fruit, 2018; USDA-ERS, 2018). There are very few large-scale viable markets for nut shells. In fact, processors have reported paying disposal fees of $11–27 per metric ton to dispose of excess shells—a direct hit to their profits. With each passing year, the worlds demand for almonds has increased, but mostly for shelled almonds (Almond Almanac, 2020), producing even more shells to be disposed. Research

---

Abbreviations: C, a constant associated with the monolayer enthalpy of sorption (–); DTG, derivative thermogravimetric; DVS, dynamic vapor sorption; FTIR, Fourier transform infrared; GAB, Guggenheim-Anderson-De Boer model; H, hard almond shells; H/C, hydrogen to carbon ratio; HHV, higher heating value; K, a constant associated with the multilayer enthalpy of sorption (–); M, equilibrium moisture content (g water/100 g dry sample); Mo, the water content in the monolayer (g water/100 g dry sample); O/C, oxygen to carbon ratio; %RH, percent relative humidity; S, soft almond shells; SS, semi-soft almond shells; T, almond twigs; TAS, torréfied almond shells; TG, thermogravimetric; TGA, thermogravimetric analysis; W, walnut shells.
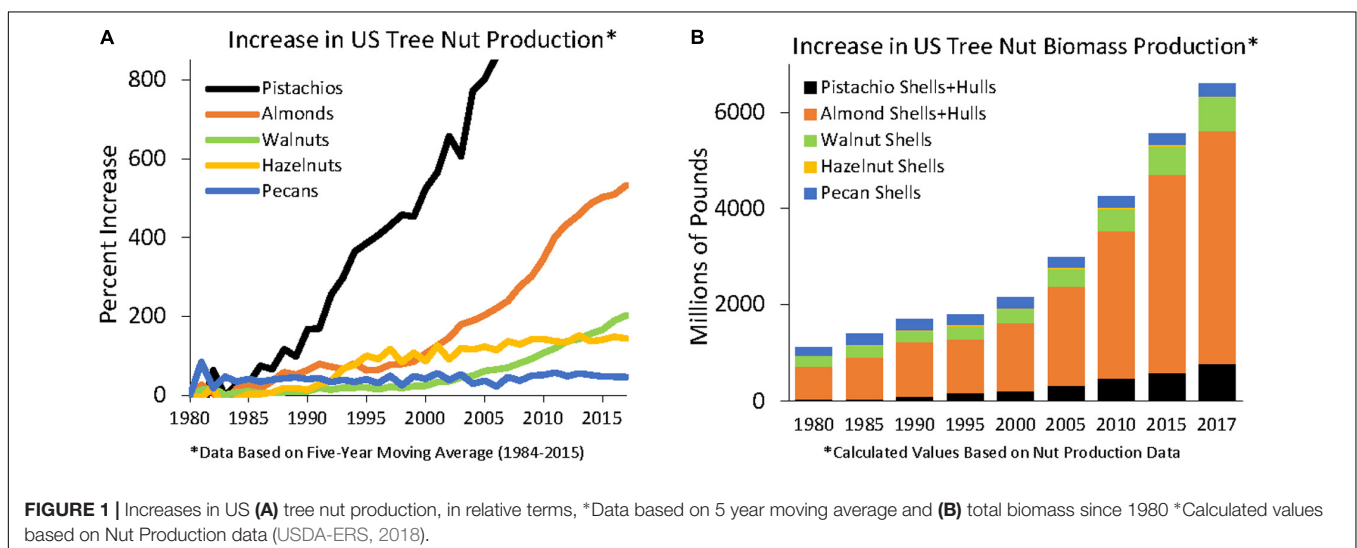
is needed to create alternate markets for these under-valued biomass feedstocks.

According to the literature there are a few studies regarding almond and walnut shells torrefaction (Arnsfeld et al., 2014; Chiou et al., 2015, 2016; Zhu et al., 2019). The mentioned manuscripts have assessed the properties of resulting torrefaction products of almond and walnut shells and the pretreatments to improve the torrefaction processes. The results indicate that torrefaction is a successful alternative to only incinerating the shells. Both almond and walnut shells present high solid and energy yields during torrefaction (Barskov et al., 2019) while maintaining low sulfur content, making it interesting to US power plants (Chiou et al., 2016). However, the torrefaction products are dependent on residence time but mostly temperature applied (Chiou et al., 2016), thus making torrefaction studies crucial to determine optimal production.

Utilization of torréfied biomass includes pretreatment for energy products (Medic et al., 2012a), soil amendment (Heikkinen et al., 2019), soil remediation (Igalavithana et al., 2017), sorbent and filtration media (Chen and Chen, 2009; Klasson et al., 2010), filler or additive in composites (McCaffrey et al., 2018), carbon black substitute (Orts, 2018), precursor for activated carbon (Zhang et al., 2016), and as a source for carbon sequestration (Craswell and Lefroy, 2001). Torrefaction is often referred to as a light pyrolysis. As shown by Das et al. (2015), biochar via pyrolysis retains much of the structural integrity of its feedstock precursor and also possesses various functional groups on its surface. This makes the product customizable for specific applications by careful selection of appropriate feedstock and varying the processing conditions. Torrefaction can produce products with similar or improved properties to biochar with lower energy inputs and lower cost (Igalavithana et al., 2017).

For energy products, torrefaction can play a significant role in decreasing transportation and storage costs of biomass needed for large scale biorefineries by improving properties prior to transport (Medic et al., 2012a). Biomass is a primary source of renewable carbon that can be utilized for biopower,

FIGURE 1 | Increases in US **(A)** tree nut production, in relative terms, *Data based on 5 year moving average and **(B)** total biomass since 1980 *Calculated values based on Nut Production data (USDA-ERS, 2018).

biofuels, and biochemicals. Currently, biomass energy accounts for the largest fraction of renewable energy sources and provides five-times more than the contribution of wind and solar to global energy consumption even with exclusion of traditional use (International Energy Agency, 2017). Torrefaction as a pretreatment process in thermochemical conversion provides the following benefits: reduced moisture of biomass resulting in improving bulk and energy density (Medic et al., 2012a; Wilk and Magdziarz, 2017); lower oxygen-to-carbon (O/C) ratio, which increases the heating value of the biomass (Wang et al., 2011); higher hydrophobicity so it maintains lower moisture content and is easier to transport and store (Hakkou et al., 2006); and improved ignitability, reactivity, and grindability so energy is saved during grinding or pulverization processes (Arias et al., 2008). Uslu et al. (2008) have reported that torrefaction has a higher process efficiency than pelletization and pyrolysis and is an important processing step that has the potential to reduce the cost of biopower and biofuels.

Utilization of torrefied biomass as a fillers in plastic composites addresses waste issues associated with both plastic and agricultural by-product (Zou et al., 2010; Arrakhiz et al., 2012; Peng et al., 2012; Chiou et al., 2016; Dikobe and Luyt, 2017; Sanjay et al., 2018). Torrefaction is used to improve the compatibility between filler and polymer by increasing the hydrophobicity of the filler (Zaghloul et al., 2017). By removing the relatively hydrophilic hemicellulose and cellulose components via torrefaction, torrefied biomass becomes increasingly hydrophobic, which improves dispersion and matrix adhesion (Berthet et al., 2016). Adding torrefied biomass residues to a polymer matrix, especially post-consumer recycled polymers, increases the value of a waste material, reduces the plastic fraction of the composite, and improves the biocomposite's mechanical and thermal properties (McCaffrey et al., 2018).

The goal of this paper was to analyze the effect of torrefaction on the properties of nut by-products. Three varieties of almond shells (hard, semi-soft, and soft), walnut shells, and almond tree trimmings were processed at two torrefaction temperatures (230 and 290°C) for three residence times (20, 40, and 60 min) to optimize physiochemical properties. Raw and treated samples were analyzed using elemental analysis, pH, bomb calorimetry, pycnometry, thermogravimetric analysis (TGA), Fourier transform infra-red (FTIR) analysis, and dynamic vapor sorption (DVS) analysis.

MATERIALS AND METHODS

Almond shells of hard, semi-soft, and soft types were a mix of California varieties as shellers and hullers do not separate shells. Almond shells and almond twigs were obtained from Almond Board of California (Modesto, CA). Walnut shells were obtained from Diamond of California (Stockton, CA). Avicel, Xylan, and lignin were purchased from Sigma Aldrich. Feedstock and chemicals were used as received.

Preparation

The raw biomass was ground to 5 mm using a Thomas Scientific Wiley knife mill (Swedesboro, NJ). Fifteen to twenty grams of raw biomass was placed in an aluminum pan (6.5 cm diameter and 1 cm height), covered with aluminum foil, and placed in a muffle furnace at ambient temperature. The furnace was purged with nitrogen gas for 30 min at flowrate of 1 liter min^{-1} prior to heating, and then heated to a set temperature of either 230 or 290°C for 20, 40, or 60 min residence time. The purge nozzle was pointed toward the back of the furnace, away from the batch vessel, to avoid disrupting the biomass. Thermocouples were placed near the floor of the furnace (referred to as oven thermocouple) and within the biomass (referred to as biomass thermocouple). The start of the residence time occurred when the oven thermocouple reached 200°C. Following torrefaction, the biomass particles were immediately cooled by placing the pan with aluminum foil cover on a steel plate at room temperature.

Elemental Composition

Elemental analysis was performed by ALS Global (Tucson, AZ) following ASTM method D3176. The elemental composition of C, H, N, and S were determined using elemental combustion analyzers LECO TruSpec Macro for C, H, and N (Joseph, MI) and ELTRA CS500 for S (Haan, Germany). The O content was determined by difference after ash determination.

Physiochemical Characteristics

Torrefied biomass yield was calculated as proportion of the torrefied product to the original raw material on a dry basis. The pH (1:20 w/v ratio using water) was measured using a HI2215 pH meter (Hanna Instruments, Woonsocket, RI). Prior to the measurement, samples were shaken for 90 min using a shaker table to ensure sufficient equilibration between solid and liquid surfaces. Higher heating value (HHV) was measured with an isoperibol calorimeter (IKA C2000, Staufen im Breisgau, Germany). Calibration was confirmed using benzoic acid standard. An AccuPyc II 1340 gas pyncnometer from Micromeritic (Norcross, GA) using helium was used for true density measurements. Reported values are the average of 5 measurements. Calibration was performed with a precision steel sphere of known volume.

Thermogravimetric Analysis (TGA)

A Perkin Elmer (Waltham, MA) Pyris 1 TGA was used to characterize the thermal stability of the samples. Each 9–11 mg sample was heated from 30 to 900°C in an alumina open crucible at a rate of 10°C/min, with nitrogen purge at a flow rate of 20 cm^3/min.

Fourier-Transform Infrared (FTIR) Spectroscopy

A Thermo Fischer Scientific Nicolet FTIR (Waltham, MA) in absorbance mode was used to perform the FTIR experiments. The IR spectrum for each sample was measured between 4,000 and 650 cm^{-1} with a resolution of 4 cm^{-1} and averaging of 16 scans. All spectra were normalized to better identify remaining peaks in harsher conditions, i.e., higher torrefaction temperature, longer residence times.

Dynamic Vapor Sorption (DVS)

Dynamic vapor sorption analysis was performed using DVS-Advantage (Surface Measurement Systems, Middlesex, United Kingdom). The instrument was used on raw and torrefed biomass samples to measure moisture uptake as a function of the relative humidity at 25.0°C. Biomass samples of 10–25 mg were placed in the sample tray for analysis. The sorption-desorption cycle used 20 steps of 90 min each, where %RH was varied stepwise from 0 to 90% then back to 0% in increments of 10%.

The isotherm data were fit to the Guggenheim-Anderson-De Boer (GAB) model, which was:

$$\frac{M}{M_o} = \frac{C\,K\,a_w}{(1 - K\,a_w)(1 - K\,a_w + C\,K\,a_w)}$$

where M is the equilibrium moisture content (g water/100 g dry sample), M_o is the water content in the monolayer (g water/100 g dry sample), C is a constant associated with the monolayer enthalpy of sorption, K is a constant associated with the multilayer enthalpy of sorption, and a_w is the water activity.

RESULTS AND DISCUSSION

Elemental Composition

Table 1 presents the experimental elemental compositions of torrefed almond [hard (H), semi-soft (SS), and soft (S)], walnut (W), and almond twigs (T) samples produced at the specified temperature and residence time. With increasing torrefaction temperature and residence time, torrefed biomass samples showed reduced hydrogen and oxygen contents, as well as increased carbon content. The nitrogen content was minimal, but generally increased with longer residence time and higher temperature. Sulfur content was also very small. Ash contents of raw almond varieties and twigs varied from 1.94 to 2.96 percent, whereas the ash content for walnut shells was lower at 0.70 percent. These results were consistent with previous studies on wood feedstock (Chen et al., 2014b; Bach et al., 2016; Kung et al., 2019).

Figure 2 shows a van Krevelen diagram for raw and torrefed biomass samples. Higher temperatures and longer residence times caused higher ratios of carbon relative to hydrogen and oxygen (i.e., move lower and to the left on the figure), which agreed with previous studies (Heidenreich et al., 2016; Kung et al., 2019; Szwaja et al., 2019). The plots of all 5 feedstocks showed linear correlations of H/C with O/C and regression coefficients greater than 0.94. Raw feedstocks had H/C ratios near 1.4 and O/C ratios between 0.6 and 0.7, similar to many reported biomass feedstocks (Ronsse et al., 2015). The most carbonized torrefed biomass had H/C ratios of 0.5–0.7 and O/C ratios between 0.2 and 0.3, which was similar to sub-bituminous coal (Ronsse et al., 2015). As mentioned previously, this was probably due to the removal of inherent hemicellulose and amorphous cellulose in the biomass. Thus, torrefed biomass can be a viewed as a sustainable alternative fuel source.

TABLE 1 | CHNSO elemental and ash composition of raw and torrefed H, SS, S, T, W samples.

Sample ID	Temp. deg.C	Resid. Time	Ash (%)	C (%)	H (%)	N (%)	Odiff. (%)	S (%)
Hraw	Raw	0	2.38	47.64	5.66	0.30	44.02	0.03
H230-20	230	20	2.57	46.79	5.40	0.30	44.91	0.03
H230-40	230	40	3.47	60.23	4.80	0.47	31.00	0.03
H230-60	230	60	5.71	59.74	4.57	0.87	29.07	0.04
H290-20	290	20	4.60	63.86	4.76	0.52	26.23	0.03
H290-40	290	40	6.38	67.78	3.95	0.57	21.29	0.03
H290-60	290	60	7.06	68.42	3.59	0.75	20.15	0.03
SSraw	Raw	0	2.22	46.73	5.56	0.41	45.06	0.02
SS230-20	230	20	2.34	51.17	5.65	0.38	40.46	<0.03
SS230-40	230	40	4.52	59.07	4.76	0.54	31.08	0.03
SS230-60	230	60	4.66	61.12	4.48	0.57	29.14	0.03
SS290-20	290	20	2.60	50.12	5.74	0.34	41.20	<0.03
SS290-40	290	40	7.68	67.77	3.61	0.85	20.05	0.04
SS290-60	290	60	7.40	69.04	3.47	0.94	19.11	0.04
Sraw	Raw	0	2.96	46.52	5.56	0.44	44.48	0.04
S230-20	230	20	2.77	49.80	5.72	0.53	41.14	0.04
S230-40	230	40	6.76	62.01	4.69	0.83	25.66	0.05
S230-60	230	60	5.58	64.60	4.00	0.92	24.85	0.05
S290-20	290	20	10.49	63.84	3.93	0.76	20.93	0.05
S290-40	290	40	8.38	65.51	3.43	1.09	21.53	0.06
S290-60	290	60	8.54	65.65	3.39	0.95	21.42	0.05
Wraw	Raw	0	0.70	48.51	5.50	0.27	44.99	0.03
W230-20	230	20	0.70	51.31	5.86	0.15	41.94	0.03
W230-40	230	40	0.90	56.62	5.25	<0.16	37.20	0.03
W230-60	230	60	1.45	60.13	4.68	0.35	33.36	0.03
W290-20	290	20	1.25	64.19	4.99	0.25	29.29	0.03
W290-40	290	40	1.68	69.40	4.10	0.32	24.47	0.03
W290-60	290	60	1.84	68.61	3.84	0.37	25.32	0.02
Traw	Raw	0	1.94	48.64	5.70	0.49	44.18	0.05
T230-20	230	20	2.11	47.49	5.39	0.51	44.46	0.04
T230-40	230	40	4.11	53.22	4.12	0.70	37.81	0.04
T230-60	230	60	5.62	55.62	3.56	0.94	34.21	0.05
T290-20	290	20	4.27	56.66	3.92	0.90	34.21	0.04
T290-40	290	40	6.18	59.31	2.81	1.21	30.44	0.05
T290-60	290	60	6.52	67.00	2.64	1.41	22.37	0.06

Physicochemical Characteristics

Figure 3 shows temperature profiles of biomass samples during torrefaction experiments at 230 and 290°C for 60 min. The 60 min samples are shown for convenience since the 20 and 40 min samples exhibited similar behavior to the 60 min samples up to their termination. Exothermic reactions in both sets of experiments resulted in sample temperatures rising considerably above the oven set temperature.

Figure 3A shows the biomass temperature ramped up at 5–6°C per minute for the first 20 min, a steeper temperature ramp between 25 and 35 min where biomass temperature exceeds the oven temperature set point at around 30 min, and then a reduced rate after that. The walnut (W) sample showed a decline in temperature rate after 40 min. H, SS, S, W, and T samples reached a maximum of 369, 390, 332, 304, and 395°C, respectively, with twigs and SS samples reaching the highest temperatures.
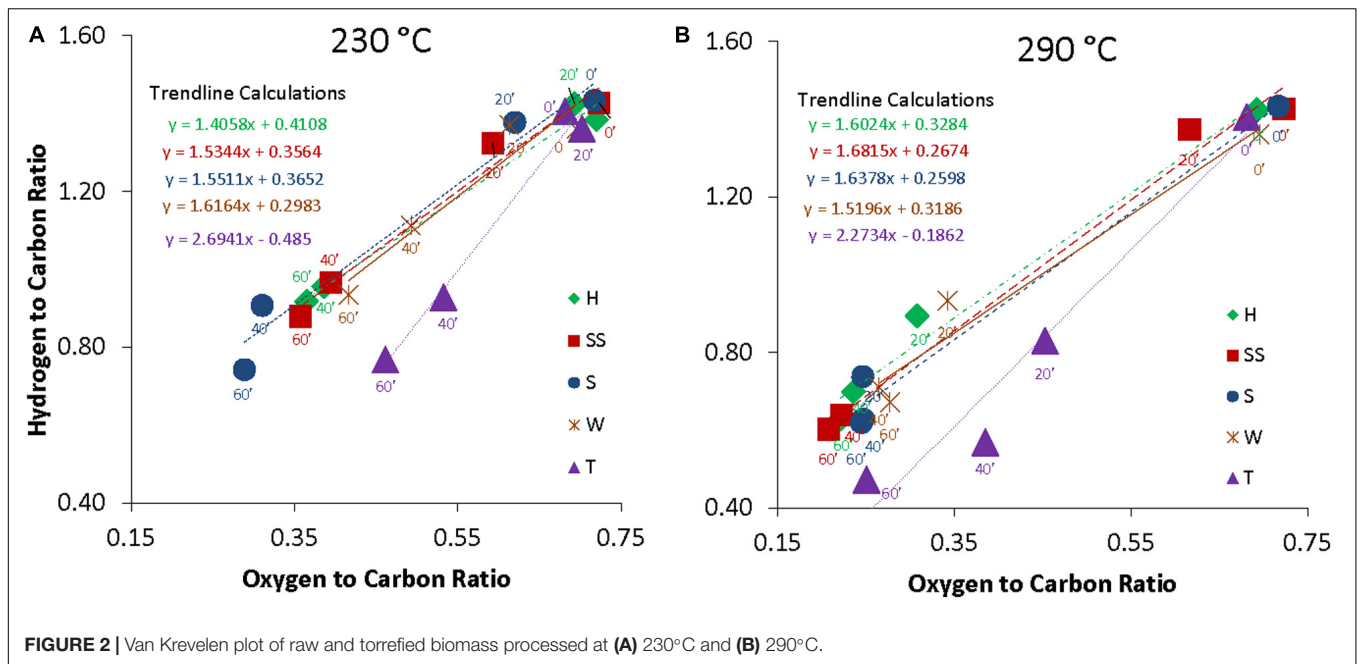
FIGURE 2 | Van Krevelen plot of raw and torrefied biomass processed at **(A)** 230°C and **(B)** 290°C.
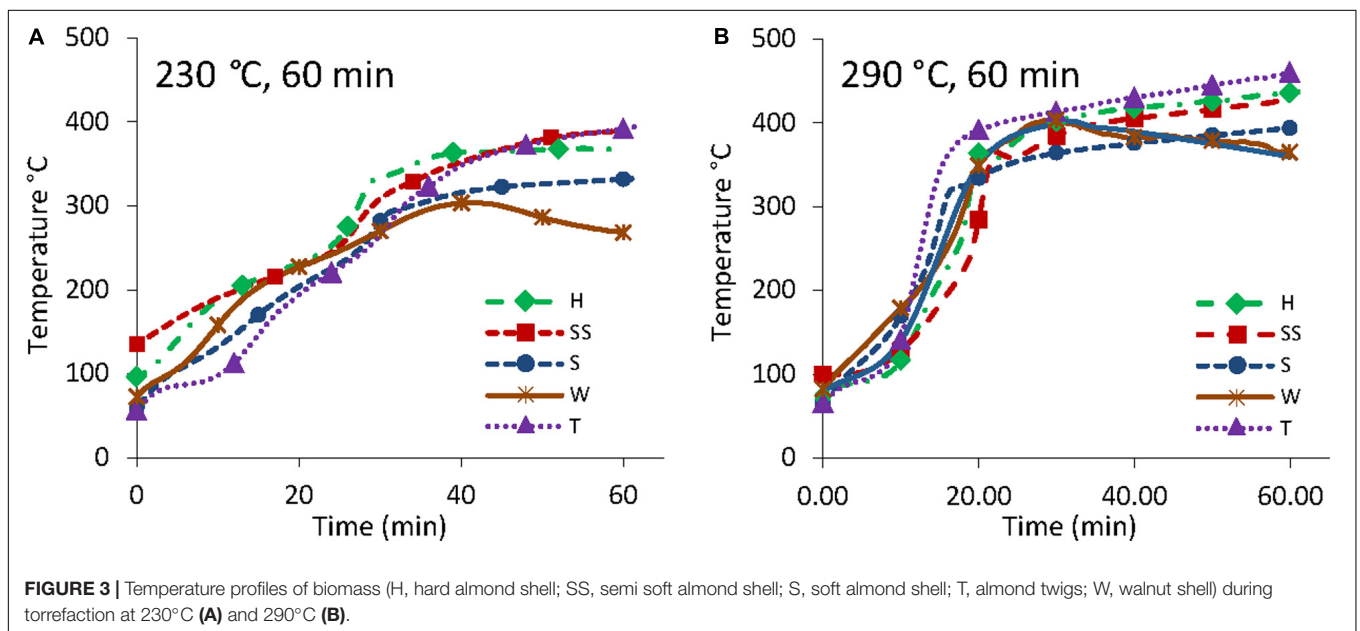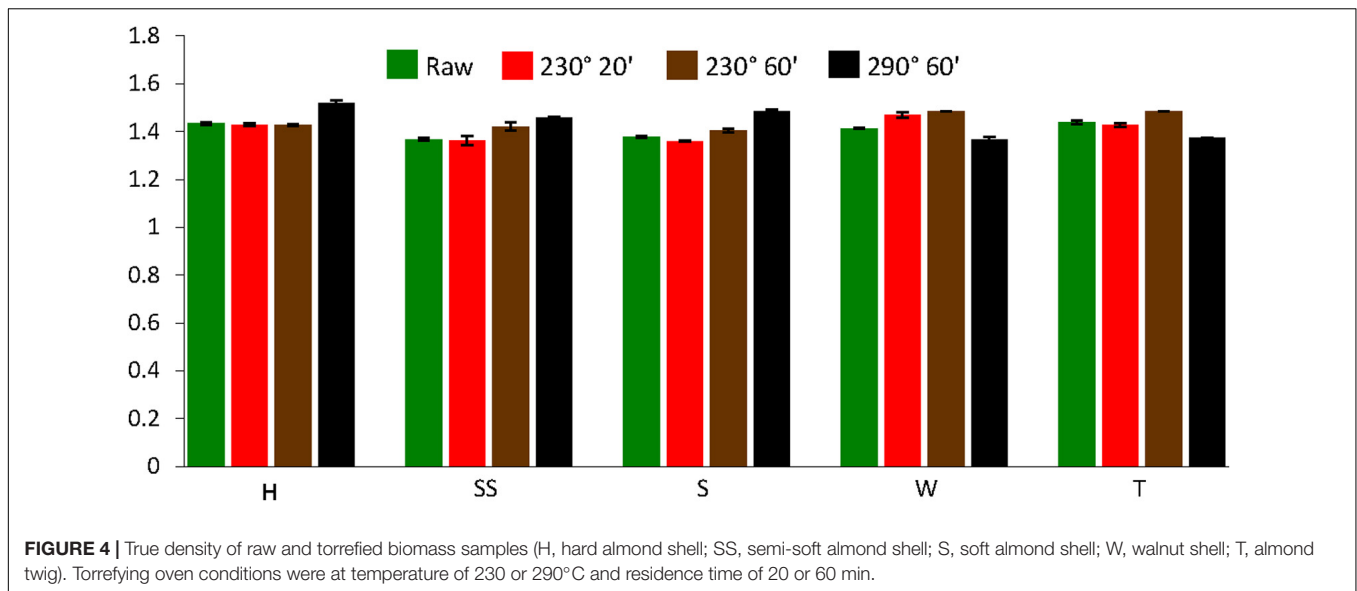

FIGURE 3 | Temperature profiles of biomass (H, hard almond shell; SS, semi soft almond shell; S, soft almond shell; T, almond twigs; W, walnut shell) during torrefaction at 230°C **(A)** and 290°C **(B)**.

Figure 3B shows the biomass temperature ramped up at 5–6°C per minute for the first 10 min, an increase to 20°C per minutes between 10 and 20 min, and then a more slow increase at 1–2°C per minute until the end of the experiment. However, walnut samples reached a maximum temperature of 403°C after 30 min and then a decline in temperature rate to 1–2°C per minute until the end of the experiment. H, SS, S, W, and T samples for the 290°C experiments reached a maximum of 437, 426, 393, 403, and 460°C, respectively, with all samples exceeding 300°C after 10 min. Temperature above 300°C suggested biomass samples experienced light pyrolysis conditions as torrefaction is typically defined as occurring in the temperature range of 200–300°C.

The observed temperature overshoot above the oven set temperature is a phenomenon that has been reported by past research (Yang et al., 2007; Chen et al., 2014a; Soponpongpipat and Sae-Ueng, 2015; Branca et al., 2016; Faleeva et al., 2018). For example, Faleeva et al. (2018) observed a temperature rise of over 150°C above the reactor set temperature in torrefaction experiments using wood feedstock in an inert atmosphere, which agrees with the current study on almond and walnut by-products. Yang et al. (2007) report that hemicellulose and lignin degradation reactions are exothermic under pyrolysis conditions while cellulose degradation is endothermic. Soponpongpipat and Sae-Ueng (2015) found that

FIGURE 4 | True density of raw and torrefied biomass samples (H, hard almond shell; SS, semi-soft almond shell; S, soft almond shell; W, walnut shell; T, almond twig). Torrefying oven conditions were at temperature of 230 or 290°C and residence time of 20 or 60 min.

compact bulk arrangement of biomass during torrefaction resulted in a higher level of degradation than a looser, less compact arrangement. Branca et al. (2016) observed temperature overshoot as high as 225°C above the reactor set temperature during pyrolysis experiments using various agriculture wastes and wood feedstock and found hazelnut shells had the greatest overshoot, followed by olive pomace, straw pellets, beech wood, and softwood (smallest overshoot) at set temperatures between 200 and 300°C.

Figure 4 shows that torrefaction did not have much of an effect on the true density of the samples. The true density of raw shells and twigs varied between 1.37 and 1.44 g/cm³, which were not significantly different than the values for torrefied samples. Previous studies on almond shells and pine chips also found that torrefaction did not significantly affect true density (Phanphanich and Mani, 2011; Chiou et al., 2016).

Table 2 shows yield, pH, and higher heating values (HHV) for the raw and torrefied biomass samples. Higher temperatures and longer residence times generally resulted in lower yields, higher pH, and larger HHV values. The minimum mass yield of the samples was 26% for W290-60. Torrefaction is known to produce yields in the range of 24–95% (Mamvura et al., 2018), so yields of 26% are not surprising given the high temperatures and long residence times. The pH values for raw feedstocks were 4.78, 4.98, 4.99, 5.16, and 6.19 for S, W, SS, T, and H, respectively. Samples torrefied at 290°C for 60 min resulted in samples with the highest pH with values of 6.90, 7.86, 9.30, 9.43, and 9.80 for T, W, SS, H, and S, respectively. The trend in pH values is probably due to the removal of inherent hemicellulose and organic acids from the biomass.

Comparing the raw samples of all feedstock to the 230–20 samples, yield changed by less than 5% (except for S) and HHV increased by less than 1%, which is not a significant change. Between 230-20 and 230-40 samples, yield changed by 24–40% and heating values increased by 22–34% over the raw heating value. Samples torrefied at 230°C for 40 min might be ideal for energy applications as heating value is significantly improved and 70–85% of the initial energy content is retained.

TABLE 2 | Yield, pH, and higher heating value (HHV) for raw and treated biomass samples.

Sample ID	% Yield	pH	HHV (MJ/kg)	SampleID	% Yield	PH	HHV (MJ/kg)
Hraw	100	6.19	19.310	Traw	100	5.16	19.850
H230-20	96.4	6.23	19.326	T230-20	97.1	5.07	20.231
H230-40	68.5	7.92	23.768	T230-40	73.1	6.11	23.606
H230-60	53.5	7.98	23.807	T230-60	57.8	6.09	23.863
H290-20	50.8	6.70	24.841	T290-20	56.0	5.36	26.559
H290-40	40.8	9.32	27.103	T290-40	42.6	6.90	27.965
H290-60	34.4	9.43	26.910	T290-60	38.1	6.90	28.660
Ssraw	100	4.99	18.577	Wraw	100	4.98	19.076
SS230-20	93.4	7.42	18.934	W230-20	95.6	5.19	19.300
SS230-40	56.5	8.30	23.952	W230-40	55.3	6.06	23.363
SS230-60	52.7	9.61	24.927	W230-60	49.5	6.29	23.148
SS290-20	48.3	9.08	26.983	W290-20	46.9	6.82	24.214
SS290-40	38.0	9.31	27.120	W290-40	34.5	6.84	25.088
SS290-60	34.3	9.30	27.232	W290-60	26.0	7.86	24.085
Sraw	100	4.78	18.588				
S230-20	81.4	5.91	19.082				
S230-40	48.1	9.30	24.905				
S230-60	44.2	8.94	25.543				
S290-20	51.3	9.69	26.410				
S290-40	40.9	8.95	26.751				
S290-60	36.2	9.86	27.066				

Thermal Analysis (TGA)

The three main components of biomass are hemicellulose, cellulose, and lignin. The properties of these major biomass components significantly affect the characteristics of torrefaction product of the biomass feedstock. Isolated thermal analysis of the individual components can provide insight to how each component behaves during torrefaction. The thermogravimetric (TG) and derivative TG (DTG) curves of cellulose (Avicel), hemicellulose (Xylan), and lignin over the temperature range of 40–900°C showed the effects of moisture loss and thermal decomposition (**Figure 5**). The first decrease of the TG curve for all 3 lignocellulosic components occurred due to moisture loss. From the DTG curve, hemicellulose degradation began at 230 °C and had two peaks at 250 and 290°C. The first peak at 250°C was due to acetyl fragmentation reactions to form acetic acid (Peng and Wu, 2010) and the second peak at 290°C was due to depolymerization reactions to form furan ring compounds, such as furfural (Collard and Blin, 2014).

At the upper torrefaction temperature limit of 300°C (Chen and Kuo, 2011), hemicellulose showed the most degradation (with 55% mass remaining), lignin showed relatively little degradation (with 87% mass remaining), and cellulose showed almost no degradation (with 99% remaining). From **Figure 3**, our biomass samples experienced temperatures over 400°C due to exothermic reactions from hemicellulose degradation, and this is confirmed by DTG analysis in **Figure 5** as well as from previous studies (Yang et al., 2007; Chen et al., 2014a; Faleeva et al., 2018). Between 300 and 400°C, hemicellulose showed lower degradation rate (with 37% mass remaining at 400°C), cellulose showed significantly more degradation (with 11% mass remaining at 400°C), and lignin showed continued degradation at a relatively slow rate (with 72% mass remaining at 400°C).

Figure 6 shows the TG curves for raw and torrefied samples (230 and 290°C for residence times of 20, 40, and 60 min). Raw H, SS, S, and W samples experienced mass losses of approximately 75%, whereas T samples showed mass losses as high as 90%. TG curves of the most heavily treated samples (290°C for 60 min) appeared similar to the TG curve of lignin from **Figure 5**. This indicated that most of the hemicellulose and cellulose had been removed via the torrefaction process. Hard shell samples torrefied at 290°C for 40 and 60 min had comparable TG curves, indicating the two samples had similar compositions and torrefaction for 40 min was sufficient. Elemental composition, pH, and HHV data of these two samples confirmed the results (**Tables 1, 2**). In contrast, almond twig samples torrefied at 290°C for 40 and 60 min showed significant differences in their TG curves, elemental compositions, and HHV values.

FTIR

Figure 7 presents FTIR spectra of Avicel (cellulose), xylan (hemicellulose), lignin, and raw walnut sample. The spectrum of raw walnut was similar to the other raw samples, only varying the intensity of the peaks. Thus, any of those could be chosen to highlight the peaks presented in these lignocellulosic materials. The spectra were divided in peaks higher than $2,700$ cm^{-1}, often assigned to intermolecular bonding, methyl groups, binding water, and carbohydrates structures, and lower than $1,750$ cm^{-1}, which was the fingerprint region (Lv et al., 2015).

From $2,800$ to $3,000$ cm^{-1}, C-H stretch vibrations were assigned to methyl, methylene, and methyne groups in all three basic constituents of the raw material (Zhao et al., 2014). A large halo at $3,200$ represented O-H stretching vibrations and could be correlated to either presence of hydroxyl groups, in all three
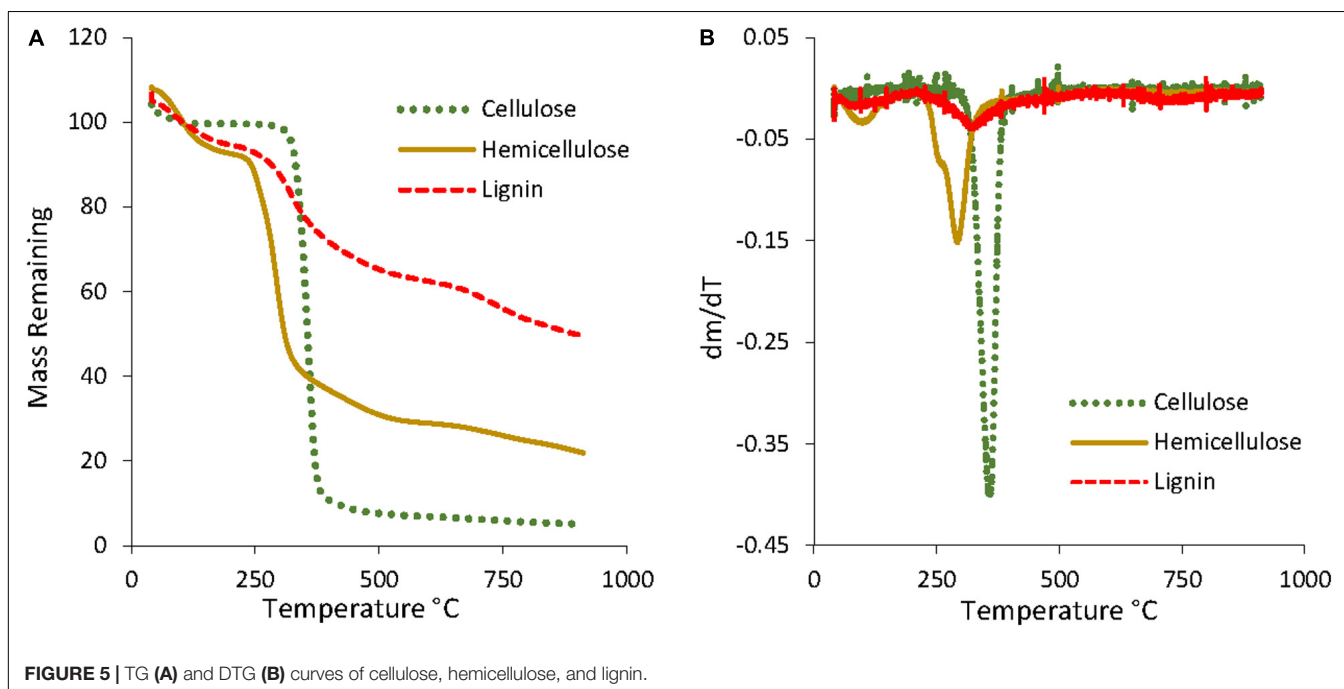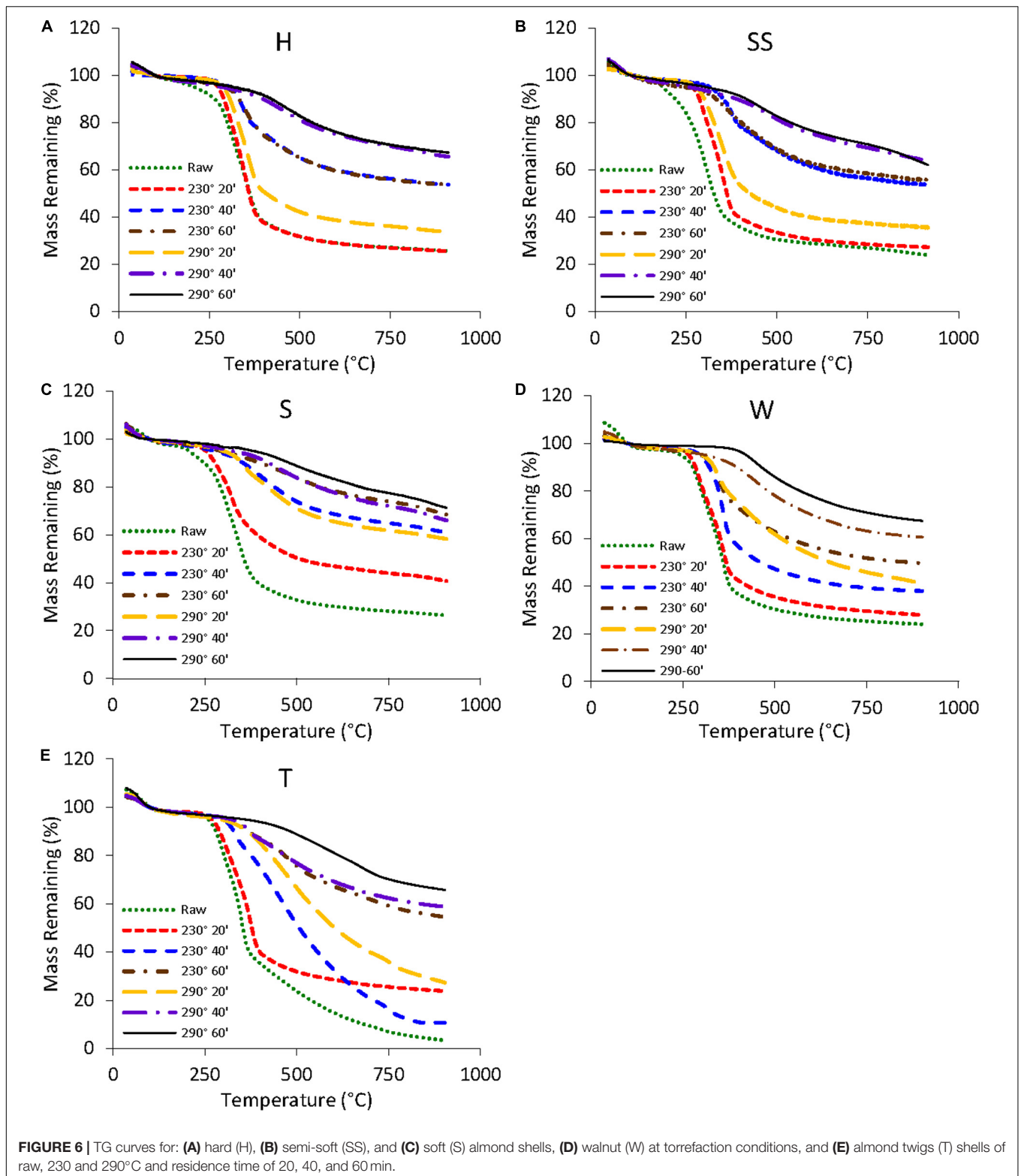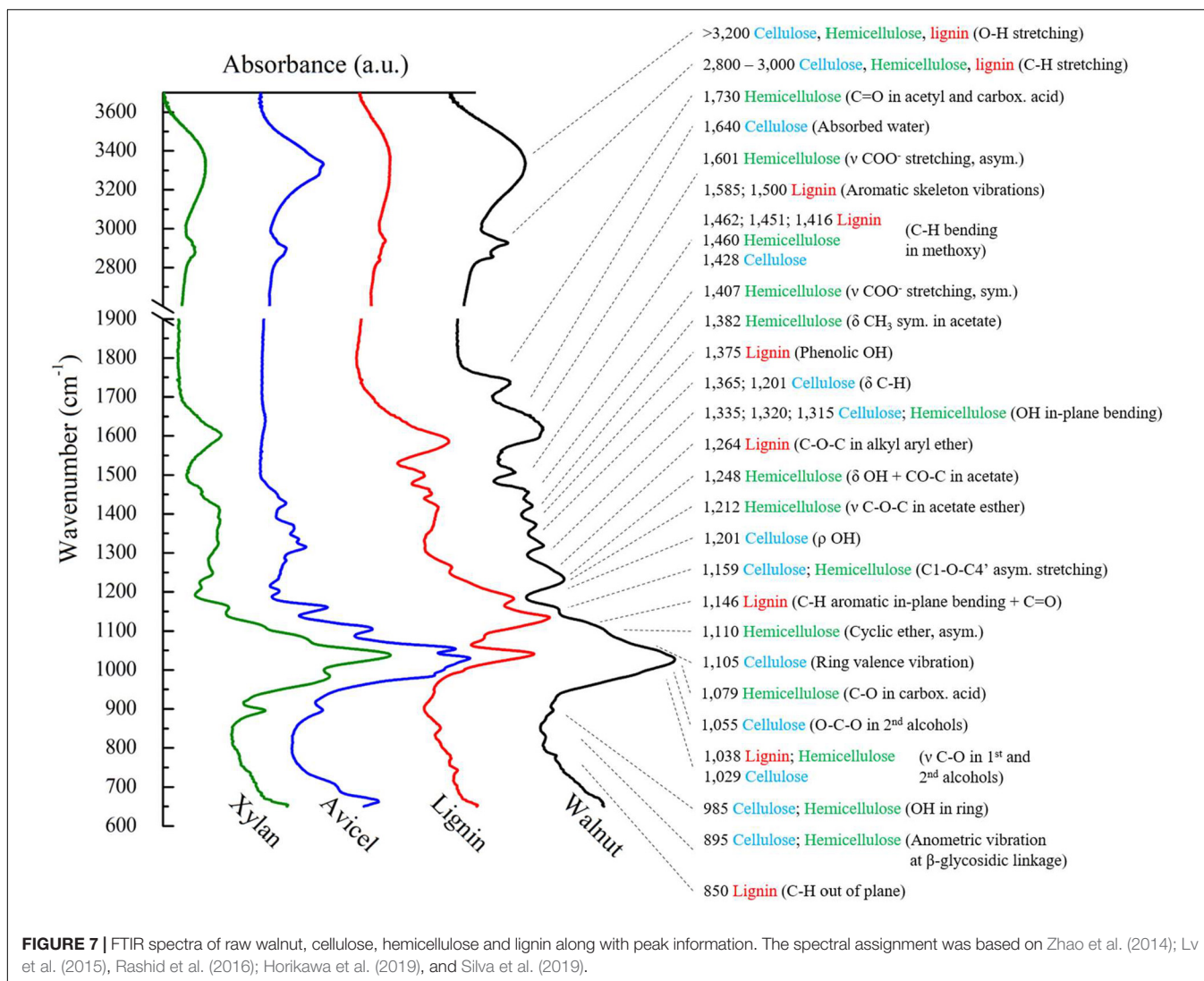

FIGURE 5 | TG **(A)** and DTG **(B)** curves of cellulose, hemicellulose, and lignin.

FIGURE 6 | TG curves for: **(A)** hard (H), **(B)** semi-soft (SS), and **(C)** soft (S) almond shells, **(D)** walnut (W) at torrefaction conditions, and **(E)** almond twigs (T) shells of raw, 230 and 290°C and residence time of 20, 40, and 60 min.

components, or hydrogen bonding, mostly in cellulose and hemicellulose (Lv et al., 2015; Silva et al., 2019).

In the fingerprint region, there were many peaks assigned to each component of the samples. Lignin contributed with

peaks related to aromatic, alcohols, and phenolic structures, Hemicellulose contained acetate, ether, and carboxylic acid functional groups, while cellulose exhibited its linear structure with alcohols and methoxy groups. A large peak around

FIGURE 7 | FTIR spectra of raw walnut, cellulose, hemicellulose and lignin along with peak information. The spectral assignment was based on Zhao et al. (2014); Lv et al. (2015), Rashid et al. (2016); Horikawa et al. (2019), and Silva et al. (2019).

1,029 cm^{-1} comprised of aromatic structure of lignin, but mostly related to the glycosidic ring vibrations of both cellulose and hemicellulose (Silva et al., 2019).
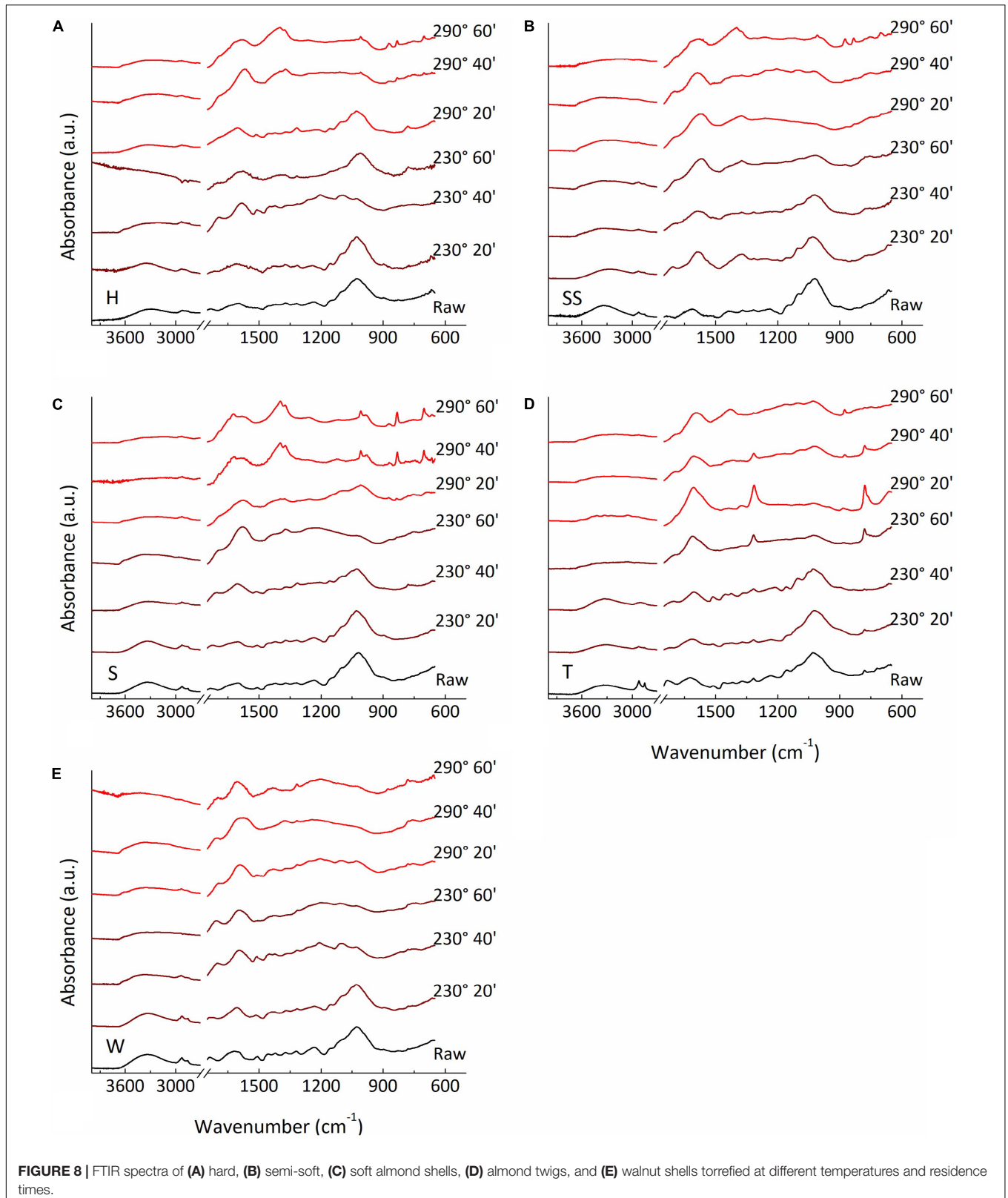
Raw samples and torrection samples at different temperatures and residence time are shown in **Figure 8**. At lower temperature and residence time (230°C, 20 min), all samples presented spectra similar to their respective raw sample, indicating that very little of its constituents had yet decomposed. Increasing either temperature or residence time had started the degradation of mainly cellulose and hemicellulose. The characteristic peak from 900 to 1,150 cm^{-1} decreased in intensity, indicating the opening of the glycoside ring, incurred from depolymerization of cellulose and hemicellulose, as well as the considerable decrease of the contribuitions from C-H and O-H stretching vibrations at higher wavenumbers. At higher temperatures and residence times, the dehydration of cellulose and hemicellulose, along with partial degradation of lignin, produced a large amount of unsaturated ketones, aldehydes and carboxylic acid salts, shown at the broad peak at 1,600 and 1,400 cm^{-1} (Lv et al., 2015). For all samples,

230°C and 60 min residence time spectra were fairly close to 290°C and 20 min, showing that the samples structure are more sensitive to temperature than residence time.

With harsher conditions, phenolic gasses produced during torrefaction started to be deposit onto the samples, showed at around 1,370 and 1,330 cm^{-1} (Zhao et al., 2014), and some characteristic peaks from lignin becomes more intense, such as aromatic skeleton vibrations at 1,585 cm^{-1} (**Figure 7**). Both vibrations are merged to the production of salts and unsatured ketones and alehydes derived from the decomposition of the samples. Thus, in order to mantaing the integrity of the samples after torrefaction and reduce energy consumption, lower temperatures and residence times should be chosen.

Dynamic Vapor Sorption

The raw biomass samples generally had higher equilibrium moisture contents than the torrefied biomass samples, especially at higher relative humidity. This is shown in **Figures 9**, **10**, which shows the sorption and desorption isotherms for all samples.

FIGURE 8 | FTIR spectra of **(A)** hard, **(B)** semi-soft, **(C)** soft almond shells, **(D)** almond twigs, and **(E)** walnut shells torrefied at different temperatures and residence times.

For raw samples, the almond shells had the highest moisture contents during the sorption cycle, whereas the walnut shell had the lowest content. Also, all almond shells had comparable moisture contents over the experimental relative humidity range. The samples torrefied at 230°C had lower moisture contents than the raw samples, with samples torrefied at longer times
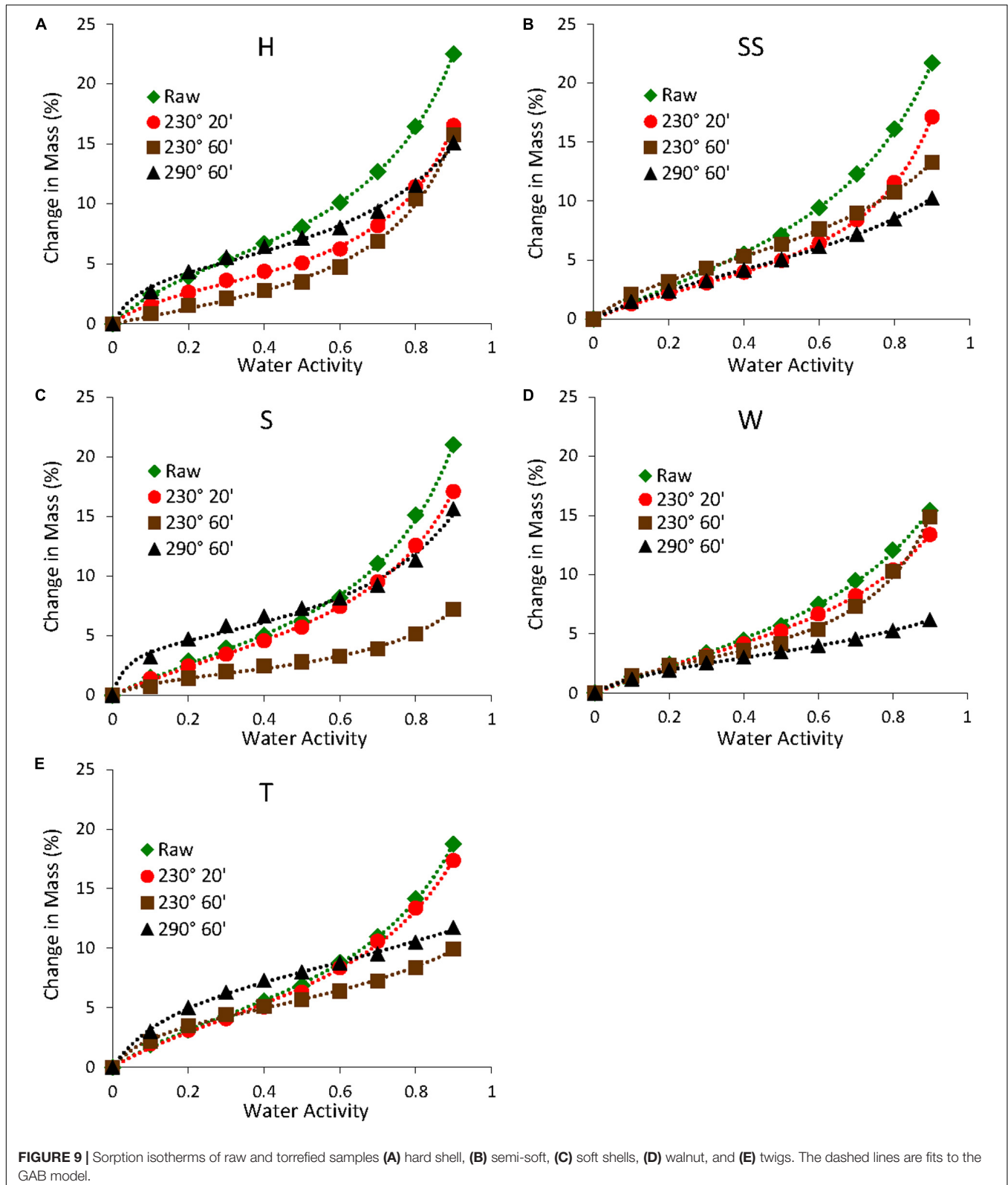
FIGURE 9 | Sorption isotherms of raw and torrefied samples **(A)** hard shell, **(B)** semi-soft, **(C)** soft shells, **(D)** walnut, and **(E)** twigs. The dashed lines are fits to the GAB model.

having even lower moisture contents. This was due in part to the degradation of hemicellulose during torrefaction, which reduced the number of hydroxyl groups that served as water binding sites (Medic et al., 2012b; Chen et al., 2014c). This was consistent with the decrease in O and H contents (**Table 1**) as well as the decrease in the absorbance of the O-H stretching region (3,200 cm^{-1}
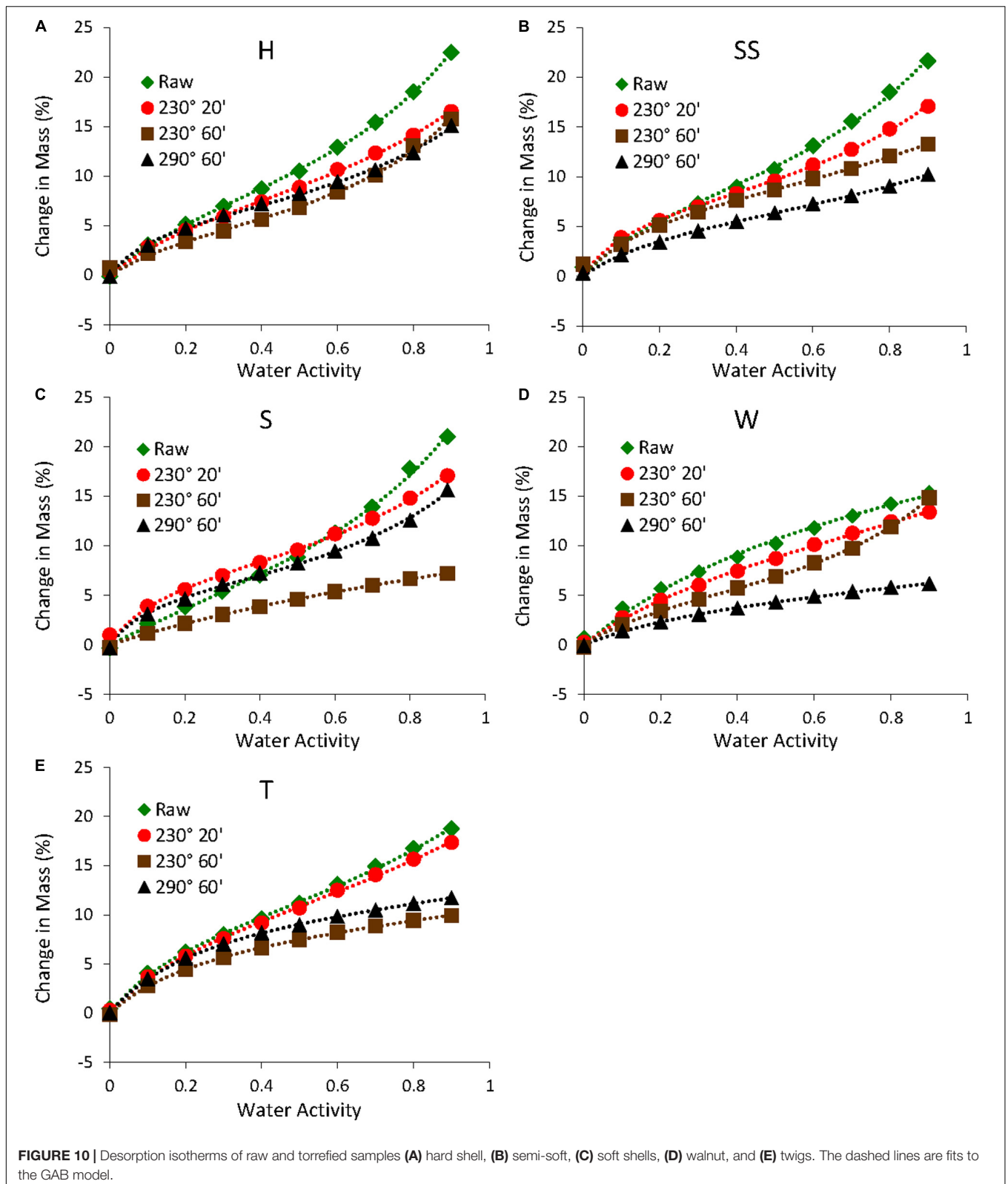
FIGURE 10 | Desorption isotherms of raw and torrefied samples **(A)** hard shell, **(B)** semi-soft, **(C)** soft shells, **(D)** walnut, and **(E)** twigs. The dashed lines are fits to the GAB model.

in **Figure 8**) for the torrefied samples. However, some samples torrefied at 290°C had higher moisture contents than samples torrefied at 230°C. This might be due to the formation of more pores during torrefaction at higher temperatures (Felfi et al., 2005), resulting in more water uptake inside the pores. Also, the degradation of crystalline cellulose at higher temperatures

TABLE 3 | GAB parameter and R^2 values for raw and torrefied samples.

Sample ID	M_o	C	K	R^2
Hraw (sorption)	5.79	6.48	0.839	1.000
Hraw (desorption)	9.46	5.37	0.692	1.000
H230-20 (sorption)	3.32	8.19	0.896	0.999
H230-20 (desorption)	8.56	6.23	0.605	0.999
H230-60 (sorption)	3.21	2.17	0.907	0.997
H230-60 (desorption)	5.56	5.98	0.753	0.995
H290-60 (sorption)	4.73	17.92	0.766	0.996
H290-60 (desorption)	6.40	12.07	0.660	0.999
SSraw (sorption)	7.02	2.55	0.800	1.000
SSraw (desorption)	9.58	6.43	0.671	0.997
SS230-20 (sorption)	3.58	4.63	0.892	1.000
SS230-20 (desorption)	6.15	10.67	0.728	0.999
SS230-60 (sorption)	5.14	7.24	0.712	1.000
SS230-60 (desorption)	8.56	11.21	0.473	0.989
SS290-60 (sorption)	4.77	5.26	0.654	1.000
SS290-60 (desorption)	6.38	8.78	0.501	0.999
Sraw (sorption)	5.22	3.39	0.859	0.999
Sraw (desorption)	10.54	2.75	0.668	0.998
S230-20 (sorption)	4.87	3.48	0.824	1.000
S230-20 (desorption)	7.75	11.99	0.639	0.995
S230-60 (sorption)	1.79	9.70	0.842	0.997
S230-60 (desorption)	11.97	6.43	0.159	0.999
S290-60 (sorption)	4.47	33.45	0.789	0.991
S290-60 (desorption)	6.15	12.75	0.689	0.998
Wraw (sorption)	6.02	2.72	0.745	0.999
Wraw (desorption)	23.61	14.88	0.096	0.993
W230-20 (sorption)	4.71	3.79	0.763	1.000
W230-20 (desorption)	12.38	7.05	0.341	0.999
W230-60 (sorption)	2.86	7.58	0.905	0.998
W230-60 (desorption)	5.54	6.66	0.727	1.000

might have resulted in a slightly more hygroscopic material (Hill et al., 2013). In addition, all samples showed hysteresis, with samples torrefied at higher temperatures and longer times generally showing lower hysteresis (results not shown). This was consistent with a study on torrefied spruce and birch, where the authors speculated that the decrease in hysteresis was due to the more severely treated samples being less hygroscopic (Kymalainen et al., 2015).

All isotherms showed very good fits to the GAB model with R^2 values greater than 0.99. This is shown in **Figures 9**, **10** and **Table 3**, which shows the GAB model parameters for all sorption and desorption isotherms. The raw samples generally had higher Mo values than the torrefied samples, which was consistent with the isotherm data (**Figures 9**, **10**).

CONCLUSION

Almond and walnut production in the US continues to increase at a rapid rate with few large outlets for the shells. Characterization of properties of torrefied by-products was investigated primarily for energy and composite-filler type applications. Three varieties

of almond shells (hard, semi-soft, and soft), walnut shells, and almond tree trimmings were processed at two torrefaction temperatures (230 and 290°C) for three residence times (20, 40, and 60 min) to optimize physiochemical properties. With increasing torrefaction temperature and residence time, torrefied biomass samples showed increased carbon content, and reduced hydrogen and oxygen contents. A van Krevelen plot (**Figure 2**) showed linear correlations of H/C with O/C had slopes between 1.49 and 2.21 indicating the torrefaction reacted faster with hydrogen than with oxygen. Temperature profiles during torrefaction show the process is exothermic with higher temperature rates at 30 min residence time for 230°C, and at 10–25 min residence time for 290°C. TGA and temperature profiles demonstrated exothermic heat release during hemicellulose degradation which will be important to consider during torrefaction reactor design. Torrefaction did not influence the true density of the samples. Higher temperatures and longer residence times generally resulted in lower yields, higher pH, and higher HHV values. Raw biomass had higher equilibrium moisture contents than the torrefied biomass samples, especially at higher relative humidity. The samples torrefied at 230°C had lower moisture contents than the raw samples, with samples torrefied at longer times having even lower moisture contents. However, some samples torrefied at 290°C had higher equilibrium moisture contents than samples torrefied at 230°C. The temperature profiles along with TGA, yield, and HHV data can be used to inform energy applications looking to boost heating value without significant loss in yield, and filler applications looking to minimize off-gassing during compounding. TGA and FTIR data confirm torrefaction removes moisture first, then hemicellulose, followed by cellulose, and mostly only lignin remained for the most processed samples.

DATA AVAILABILITY STATEMENT

The original contributions presented in the study are included in the article/supplementary material, further inquiries can be directed to the corresponding author/s.

AUTHOR CONTRIBUTIONS

ZM, LT, B-SC, DW, and WO conceived of the presented idea. ZM and LT performed the experiments. DW and WO verified the analytical methods. LS and SF analyzed FTIR results. B-SC analyzed DVS results. All authors discussed the results and contributed to the final manuscript.

ACKNOWLEDGMENTS

REFERENCES

Almond Almanac (2020). Available online at: https://www.almonds.com/sites/default/files/2020-12/2020%20Almond%20Almanac.pdf (accessed February 2, 2021)

Almond Board of California (2018). *Almond Almana*. Modesto, CA: Almond Board of California.

Arias, B., Pevida, C., Fermoso, J., Plaza, M. G., Rubiera, F., and Pis, J. J. (2008). Influence of torrefaction on the grindability and reactivity of woody biomass. *Fuel Process. Technol.* 89, 169–175. doi: 10.1016/j.fuproc.2007.09.002

Arnsfeld, S., Senk, D., and Gudenau, H.-W. (2014). The qualification of torrefied wooden biomass and agricultural wastes products for gasification processes. *J. Anal. Appl. Pyrol.* 107, 133–141. doi: 10.1016/j.jaap.2014.02.013

Arrakhiz, F. Z., El Achaby, M., Benmoussa, K., Bouhfid, R., Essassi, E. M., and Qaiss, A. (2012). Evaluation of mechanical and thermal properties of Pine cone fibers reinforced compatibilized polypropylene. *Mater. Des.* 40, 528–535. doi: 10.1016/j.matdes.2012.04.032

Bach, Q., Chen, W., Chu, Y., and Skreiberg, O. (2016). Predictions of biochar yield and elemental composition during torrefaction of forest residues. *Bioresour. Technol.* 215, 239–246. doi: 10.1016/j.biortech.2016.04.009

Barskov, S., Zappi, M., Buchireddy, P., Dufreche, S., Guillory, J., Gang, D., et al. (2019). Torrefaction of biomass: a review of production methods for biocoal from cultured and waste lignocellulosic feedstocks. *Renew. Energy* 142, 624–642. doi: 10.1016/j.renene.2019.04.068

Berthet, M. A., Commandré, J.-M., Rouau, X., Gontard, N., and Coussy, H. (2016). Torrefaction treatment of lignocellulosic fibres for improving fibre/matrix adhesion in a biocomposite. *Mater. Des.* 92, 223–232. doi: 10.1016/j.matdes.2015.12.034

Branca, C., Di Blasi, C., and Galgano, A. (2016). Chemical characterization of volatile products of biomass pyrolysis under significant reaction-induced overheating. *J. Anal. Appl. Pyrol.* 119, 8–17. doi: 10.1016/j.jaap.2016.04.004

Chen, B., and Chen, Z. (2009). Sorption of naphthalene and 1-naphthol by biochars of orange peels with different pyrolytic temperatures. *Chemosphere* 76, 127–133. doi: 10.1016/j.chemosphere.2009.02.004

Chen, D., Gao, A., Ma, Z., Fei, D., Chang, Y., and Shen, C. (2018). In-depth study of rice husk torrefaction: characterization of solid, liquid and gaseous products, oxygen migration and energy yield. *Bioresour. Technol.* 253, 148–153. doi: 10.1016/j.biortech.2018.01.009

Chen, W. H., Kuo, P., Liu, S., and Wu, W. (2014a). Thermal characterization of oil palm fiber and eucalyptus in torrefaction. *Energy* 71, 40–48. doi: 10.1016/j.energy.2014.03.117

Chen, W.-H., and Kuo, P.-C. (2011). Torrefaction and co-torrefaction characterization of hemicellulose, cellulose, and lignin as well as torrefaction of some basic constituents in biomass. *Energy*, 36, 803–811.

Chen, W. H., Lu, K., Lee, W., Liu, S., and Lin, T. (2014b). Non-oxidative and oxidative torrefaction characterization and SEM observations of fibrous and ligneous biomass. *Appl. Energy* 114, 104–113. doi: 10.1016/j.apenergy.2013.09.045

Chen, Y., Liu, B., Yang, H., Yang, Q., and Chen, H. (2014c). Evolution of functional groups and pore structure during cotton and corn stalks torrefaction and its correlation with hydrophobicity. *Fuel* 137, 41–49. doi: 10.1016/j.fuel.2014.07.036

Chiou, B.-S., Valenzuela-Medina, D., Bilbao-Sainz, C., Klamczynski, A. P., Avena-Bustillos, R. J., Milczarek, R. R., et al. (2016). Torrefaction of almond shells: effects of torrefaction conditions on properties of solid and condensate products. *Ind. Crops Prod.* 86, 40–48. doi: 10.1016/j.indcrop.2016.03.030

Chiou, B.-S., Valenzuela-Medina, D., Wechsler, M., Bilbao-Sainz, C., Klamczynski, A. K., Williams, T. G., et al. (2015). Torrefied biomass-polypropylene composites. *J. Appl. Polym. Sci.* 132, 1–8.

Collard, F., and Blin, J. (2014). A review on pyrolysis of biomass constituents: mechanisms and composition of the products obtained from the conversion of cellulose, hemicelluloses and lignin. *Renew. Sustain. Energy Rev.* 38, 594–608. doi: 10.1016/j.rser.2014.06.013

Craswell, E., and Lefroy, R. (2001). The role and function of organic matter in tropical soils. *Nutr. Cycl. Agroecosyst.* 61:7. doi: 10.1007/978-94-017-2172-1_2

Das, O., Sarmah, A., and Bhattacharyya, D. (2015). A sustainable and resilient approach through biochar addition in wood polymer composites. *Sci. Tot. Environ.* 512–513, 326–336. doi: 10.1016/j.scitotenv.2015.01.063

Dikobe, D. G., and Luyt, A. S. (2017). Thermal and mechanical properties of PP/HDPE/wood powder and MAPP/HDPE/wood powder polymer blend composites. *Thermochim. Acta* 654, 40–50. doi: 10.1016/j.tca.2017.05.002

Doddapaneni, K., Jain, R., Praveenkumar, R., Rintala, J., Romar, H., and Konttinen, J. (2018). Adsorption of furfural from torrefaction condensate using torrefied biomass. *Chem. Eng. J.* 334, 558–568. doi: 10.1016/j.cej.2017.10.053

Fagernas, L., Kuoppala, E., and Arpiainen, V. (2015). Composition, utilization, and economic assessment of torrefaction condensates. *Energy Fuels* 29, 3134–3142. doi: 10.1021/acs.energyfuels.5b00004

Faleeva, J. M., Sinelshchikov, V. A., Sytchev, G. A., and Zaichenko, V. M. (2018). Exothermic effect during torrefaction. *J. Phys.* 946:012033. doi: 10.1088/1742-6596/946/1/012033

Felfi, F. F., Luengo, C. A., Suarez, J. A., and Beaton, P. A. (2005). Wood briquette torrefaction. *Energy Sustain. Dev.* 9, 19–22. doi: 10.1016/s0973-0826(08)60519-0

Fuad, M. A. H. M., Hasan, M. F., and Ani, F. N. (2019). Microwave torrefaction for viable fuel production: a review on theory, affecting factors, potential and challenges. *Fuel* 253, 512–526. doi: 10.1016/j.fuel.2019.04.151

Hakkou, M., Pétrissans, M., Gérardin, P., and Zoulalian, A. (2006). Investigations of the reasons for fungal durability of heat-treated beech wood. *Polym. Degrad. Stab.* 91, 393–397. doi: 10.1016/j.polymdegradstab.2005.04.042

Heidenreich, S., Müller, M., and Foscolo, P. (2016). "Chapter 3 – Biomass pretreatment," in *Advanced Biomass Gasification*, eds S. Heidenreich, M. Müller, and P. U. Foscolo (Cambridge, MA: Academic Press), 11–17.

Heikkinen, J., Keskinen, R., Soinne, H., Hyväluoma, J., Nikama, J., Wikberg, H., et al. (2019). Possibilities to improve soil aggregate stability using biochars derived from various biomasses through slow pyrolysis, hydrothermal carbonization, or torrefaction. *Geoderma* 344, 40–49. doi: 10.1016/j.geoderma.2019.02.028

Hill, S. J., Grigsby, W. J., and Hall, P. W. (2013). Chemical and cellulose crystallite changes in *Pinus radiata* during torrefaction. *Biomass Bioenergy* 56, 92–98. doi: 10.1016/j.biombioe.2013.04.025

Horikawa, Y., Hirano, S., Mihashi, A., Kobayashi, Y., Zhai, S., and Sugiyama, J. (2019). Prediction of Lignin contents from infrared spectroscopy: chemical digestion and Lignin/Biomass ratios of *Cryptomeria japonica*. *Appl. Biochem. Biotechnol.* 188, 1066–1076. doi: 10.1007/s12010-019-02965-8

Igalavithana, A. D., Lee, S. E., Lee, Y. H., Tsang, D., Rinklebe, J., Kwon, E. E., et al. (2017). Heavy metal immobilization and microbial community abundance by vegetable waste and pine cone biochar of agricultural soils. *Chemosphere* 174, 593–603. doi: 10.1016/j.chemosphere.2017.01.148

International Energy Agency (2017). *Technology Roadmap: Delivering Sustainable Bioenergy*. Paris: International Energy Agency.

International Nuts & Dried Fruit (2018). *Statistical Yearbook 2018/19*. Reus: International Nuts & Dried Fruit.

Klasson, K. T., Ledbetter, C. A., Wartelle, L. H., and Lingle, S. E. (2010). Feasibility of dibromochloropropane (DBCP) and trichloroethylene (TCE) adsorption onto activated carbons made from nut shells of different almond varieties. *Ind. Crops Prod.* 31, 261–265. doi: 10.1016/j.indcrop.2009.11.002

Kung, K., Thengane, S., Shanbhogue, S., and Ghoniem, A. (2019). Parametric analysis of torrefaction reactor operating under oxygen lean conditions. *Energy* 181, 603–614. doi: 10.1016/j.energy.2019.05.194

Kymalainen, M., Rautkari, L., and Hill, C. A. S. (2015). Sorption behavior of torrefied wood and charcoal determined by dynamic vapour sorption. *J. Mater. Sci.* 50, 7673–7680. doi: 10.1007/s10853-015-9332-2

Lv, P., Almeida, G., and Perré, P. (2015). TGA-FTIR analysis of terrefaction of lignocellulosic components (cellulose, xylan, lignin) in isothermal conditions over a wide range of time durations. *BioResources* 10, 4239–4251.

Mamvura, T. A., Pahla, G., and Muzenda, E. (2018). Torrefaction of waste biomass for application in energy production in South Africa. *S. Afr. J. Chem. Eng.* 25, 1–12. doi: 10.1016/j.sajce.2017.11.003

McCaffrey, Z., Torres, L., Flynn, S., Cao, T., Chiou, B.-S., Klamczynski, A., et al. (2018). Recycled polypropylene-polyethylene torrefied almond shell biocomposites. *Ind. Crops Prod.* 125, 425–432. doi: 10.1016/j.indcrop.2018.09.012

Medic, D., Darr, M., Shah, A., Potter, B., and Zimmerman, J. (2012a). Effects of torrefaction process parameters on biomass feedstock upgrading. *Fuel* 91, 147–154. doi: 10.1016/j.fuel.2011.07.019

Medic, D., Darr, M., Shah, A., and Rahn, S. (2012b). Effect of torrefaction on water vapor adsorption properties and resistance to microbial degradation of corn stover. *Energy Fuels* 26, 2386–2393. doi: 10.1021/ef3000449

Melkior, T., Jacob, S., Gerbaud, G., Hediger, S., Le Pape, L., Bonnefois, L., et al. (2012). NMR analysis of the transformation of wood constituents by torrefaction. *Fuel* 92, 271–280. doi: 10.1016/j.fuel.2011.06.042

Orts, W. (2018). *Application and Production of Black Carbon from Almond Shells*. Sacramento, CA: Almond Conference.

Peng, J. H., Bi, H. T., Sokhansanj, S., and Lim, J. C. (2012). A study of particle size effect on biomass torrefaction and densification. *Energy Fuels* 26, 3826–3839. doi: 10.1021/ef3004027

Peng, Y., and Wu, S. (2010). The structural and thermal characteristics of wheat straw hemicellulose. *J. Anal. Appl. Pyrol.* 88, 134–139. doi: 10.1016/j.jaap.2010.03.006

Phanphanich, M., and Mani, S. (2011). Impact of torrefaction on the grindability and fuel characteristics of forest biomass. *Bioresour. Technol.* 102, 1246–1253. doi: 10.1016/j.biortech.2010.08.028

Rashid, T., Kait, C. F., and Murugesan, T. A. (2016). Fourier Transformed Infrared" compound study of lignin recovered from a formic acid process. *Proc. Eng.* 148, 1312–1319. doi: 10.1016/j.proeng.2016.06.547

Ronsse, F., Nachenius, R., and Prins, W. (2015). "Chapter 11 – Carbonization of biomass," in *Recent Advances in Thermo-Chemical Conversion of Biomass*, eds A. Pandey, T. Bhaskar, M. Stöcker, and R. Sukumaran (Amsterdam: Elsevier), 293–324.

Sanjay, M. R., Madhu, P., Jawaid, M., Senthamaraikannan, P., Senthil, S., and Pradeep, S. (2018). Characterization and properties of natural fiber polymer composites: a comprehensive review. *J. Clean. Prod.* 172, 566–581. doi: 10.1016/j.jclepro.2017.10.101

Silva, L. E., Claro, P. I. C., Sanfelice, R. C., Guimaraes, M. Jr., Oliveira, J. E., Ugucioni, J. C., et al. (2019). Cellulose nanofibrils modification with polyaniline aiming at enhancing electrical properties for application in flexible electronics. *Cellul. Chem. Technol.* 53, 775–786.

Soponpongpipat, N., and Sae-Ueng, U. (2015). The effect of biomass bulk arrangements on the decomposition pathways in the torrefaction process. *Renew. Energy* 81, 679–684. doi: 10.1016/j.renene.2015.03.060

Stelte, W. (2012). *Torrefaction of Unutilized Biomass Resources and Characterization of Torrefaction Gasses*. Taastrup: Danish Technological Institute.

Szwaja, S., Magdziarz, A., Zajemska, M., and Poskart, A. (2019). A torrefaction of Sida hermaphrodita to improve fuel properties. Advanced analysis of torrefied products. *Renew. Energy* 141, 894–902. doi: 10.1016/j.renene.2019.04.055

USDA-ERS (2018). *Fruit and Nut Tree Data*. Washington, DC: USDA-ERS.

Uslu, A., Faaij, A., and Bergman, P. (2008). Pre-treatment technologies, and their effect on international bioenergy supply chain logistics. Techno-economic evaluation of torrefaction, fast pyrolysis and pelletisation. *Energy* 33, 1206–1223. doi: 10.1016/j.energy.2008.03.007

Wang, G., Luo, Y., Deng, J., Kuang, J., and Zhang, Y. (2011). Pretreatment of biomass by torrefaction. *Chin. Sci. Bull.* 56, 1442–1448.

Wilk, M., and Magdziarz, A. (2017). Hydrothermal carbonization, torrefaction and slow pyrolysis of *Miscanthus giganteus*. *Energy* 140, 1292–1304. doi: 10.1016/j.energy.2017.03.031

Yan, B., Jiao, L., Li, J., Zhu, X., Ahmed, S., and Chen, G. (2021). Investigation on microwave torrefaction: parametric influence, TG-MS-FTIR analysis, and gasification performance. *Energy* 220:119794. doi: 10.1016/j.energy.2021.119794

Yang, H., Yan, R., Chen, H., Lee, D. H., and Zheng, C. (2007). Characteristics of hemicellulose, cellulose and lignin pyrolysis. *Fuel* 86, 12–13.

Zaghloul, M. M. Y., Zaghloul, M. Y. M., and Zaghloul, M. M. Y. (2017). Experimental and modeling analysis of mechanical-electrical behaviors of polypropylene composites filled with graphite and MWCNT fillers. *Polym. Test.* 63, 467–474. doi: 10.1016/j.polymertesting.2017.09.009

Zhang, S., Hu, B., Zhang, L., and Xiong, Y. (2016). Effects of torrefaction on yield and quality of pyrolysis char and its application on preparation of activated carbon. *J. Anal. Appl. Pyrol.* 119, 217–223. doi: 10.1016/j.jaap.2016.03.002

Zhao, J., Xiuwen, W., Hu, J., Liu, Q., Shen, D., and Xiao, R. (2014). Thermal degradation of softwood lignin and hardwood lignin by TGFTIR and Py-GC/MS. *Polym. Degrad. Stab.* 108, 133–138. doi: 10.1016/j.polymdegradstab.2014.06.006

Zhu, X., Luo, Z., Diao, R., and Zhu, X. (2019). Combining torrefaction pretreatment and co-pyrolysis to upgrade biochar derived from bio-oil distillation residue and walnut shell. *Energy Conver. Manag.* 199:111970. doi: 10.1016/j.enconman.2019.111970

Zou, Y., Huda, S., and Yang, Y. (2010). Lightweight composites from long wheat straw and polypropylene web. *Bioresour. Technol.* 101, 2026–2033. doi: 10.1016/j.biortech.2009.10.042